

## Exploring the evolution of stellar rotation using Galactic kinematics

RUTH ANGUS,<sup>1,2,3</sup> ANGUS BEANE,<sup>4</sup> ADRIAN M. PRICE-WHELAN,<sup>2</sup> JASON CURTIS,<sup>1</sup> TRAVIS BERGER,<sup>5</sup> ELISABETH NEWTON,<sup>6</sup> JENNIFER VAN SADERS,<sup>5</sup> ROCIO KIMAN,<sup>7</sup> DAN FOREMAN-MACKEY,<sup>2</sup> YUXI (LUCY) LU,<sup>3,1</sup> LAUREN ANDERSON,<sup>8</sup> AND JACQUELINE K. FAHERTY<sup>1</sup>

<sup>1</sup>Department of Astrophysics, American Museum of Natural History, 200 Central Park West, Manhattan, NY, USA

<sup>2</sup>Center for Computational Astrophysics, Flatiron Institute, 162 5th Avenue, Manhattan, NY, USA

<sup>3</sup>Department of Astronomy, Columbia University, Manhattan, NY, USA

<sup>4</sup>Center for Astrophysics — Harvard & Smithsonian, 60 Garden Street, Cambridge, MA 02138, USA

<sup>5</sup>Institute for Astronomy, University of Hawai‘i, 2680 Woodlawn Drive, Honolulu, HI 96822, USA

<sup>6</sup>Department of Physics and Astronomy, Dartmouth College, Hanover, NH, USA

<sup>7</sup>Department of physics, CUNY Graduate Center, City University of New York, Manhattan, NY, USA

<sup>8</sup>Observatories of the Carnegie Institution for Science, 813 Santa Barbara Street, Pasadena, CA 91101, USA

## ABSTRACT

The rotational evolution of cool dwarfs is poorly constrained after  $\sim$ 1-2 Gyr due to a lack of precise ages and rotation periods for old main-sequence stars. In this work we use velocity dispersion as an age proxy to reveal the temperature-dependent rotational evolution of low-mass *Kepler* dwarfs, and demonstrate that kinematic ages could be a useful tool for calibrating gyrochronology in the future.

We find that a linear gyrochronology model, calibrated to fit the period– $T_{\text{eff}}$  relationship of the Praesepe cluster, does not apply to stars older than around 1 Gyr. Although late-K dwarfs spin more slowly than early-K dwarfs when they are young, at old ages we find that late-K dwarfs rotate at the same rate or faster than early-K dwarfs of the same age. This result agrees qualitatively with semi-empirical models that vary the rate of surface-to-core angular momentum transport as a function of time and mass. It also aligns with recent observations of stars in the NGC 6811 cluster, which indicate that the surface rotation rates of K dwarfs go through an epoch of inhibited evolution. We find that the oldest *Kepler* stars with measured rotation periods are late-K and early-M dwarfs, indicating that these stars maintain spotted surfaces and stay magnetically active longer than more massive stars. Finally, based on their kinematics, we confirm that many rapidly rotating GKM dwarfs are likely to be synchronized binaries.

## 1. INTRODUCTION

### 1.1. Gyrochronology

Stars with significant convective envelopes ( $\lesssim 1.3 M_{\odot}$ ) have strong magnetic fields and slowly lose angular momentum via magnetic braking (e.g. Schatzman 1962; Weber & Davis 1967; Kraft 1967; Skumanich 1972; Kawaler 1988; Pinsonneault et al. 1989). Although stars are born with random rotation periods, between 1 and 10 days, observations of young open clusters reveal that their rotation periods converge onto a unique sequence by  $\sim$ 500-700 million years (e.g. Irwin & Bouvier 2009; Gallet & Bouvier 2013). After this time, the rotation period of a star is thought to be determined, to first order, by its color and age alone. This is the principle behind gyrochronology, the method of inferring a star’s age from its rotation period (e.g. Barnes 2003, 2007, 2010; Meibom et al. 2011, 2015). However, new photometric rotation periods made available by the *Kepler* (Borucki et al. 2010) and *K2* (Howell et al. 2014) missions (e.g. McQuillan et al. 2014; García et al. 2014; Douglas et al. 2017; Rebull et al. 2017; Meibom et al. 2011, 2015; Curtis et al. 2019) confirm that rotational evolution is a highly complex process. For example, the early-to-mid M dwarfs in the  $\sim$  650 Myr Praesepe cluster spin more slowly than the G dwarfs; in theory because lower-mass stars have deeper convective zones which generate stronger magnetic fields and more efficient magnetic braking. However, in the NGC

6811 cluster which is around 1 Gyr (Janes & Hoq 2011; Sandquist et al. 2016), late-K dwarfs rotate at the *same rate* as early-K dwarfs (Curtis et al. 2019). New semi-empirical models that vary the rate of angular momentum redistribution in the interiors of stars are able to reproduce this flattened period–color relation (Spada & Lanzafame 2019). These models suggest that mass and age-dependent angular momentum transport between the cores and envelopes of stars has a significant impact on their surface rotation rates.

Another example of unexpected rotational evolution is seen in old field stars which appear to rotate more rapidly than classical gyrochronology models predict (Angus et al. 2015; van Saders et al. 2016, 2018; Metcalfe & Egeland 2019). A mass-dependent modification to the classical  $P_{\text{rot}} \propto t^{\frac{1}{2}}$  spin-down law (Skumanich 1972) is required to reproduce these observations. To fit magnetic braking models to these data, a cessation of magnetic braking is required after stars reach a Rossby number ( $\text{Ro}$ ; the ratio of rotation period to convective turnover time) of around 2 (van Saders et al. 2016, 2018).

The rotational evolution of stars is clearly a complicated process and, to fully calibrate the gyrochronology relations we need a large sample of reliable ages for stars spanning a range of ages and masses. In this paper, we use the velocity dispersions of field stars to qualitatively explore the rotational evolution of GKM dwarfs, and show that kinematics could provide a gyrochronology calibration sample.

### 1.2. Using velocity dispersion as an age proxy

Stars are thought to be born in the thin disk of the Milky Way (MW), orbiting the Galaxy with a low out-of-plane, or vertical, velocity ( $v_z$ ), just like the star-forming molecular gas observed in the disk today (e.g. Stark & Brand 1989; Stark & Lee 2005; Aumer & Binney 2009; Martig et al. 2014; Aumer et al. 2016). On average, the vertical velocities of older stars is observed to be larger (e.g. Nordström et al. 2004; Holmberg et al. 2007, 2009; Aumer & Binney 2009; Casagrande et al. 2011). This is likely either a signature of dynamical heating, such as from interactions with giant molecular clouds, spiral arms and the galactic bar (see Sellwood 2014, for a review of secular evolution in the MW), or an indication that stars formed dynamically “hotter” in the past (e.g., Bird et al. 2013). In either case, the vertical velocity distribution is observed to depend significantly on stellar age. While the velocity of any individual star only provides a weak age constraint (if any at all) because its velocity depends on its current position in its orbit, the velocity dispersion of a population of stars indicates whether that population is old or young relative to other populations. In this work, we compare the velocity dispersions of populations of field stars in the Galactic thin disk to ascertain which populations are older and which younger, and draw conclusions about the rotational evolution of stars based on their implied relative ages.

Kinematic ages have been used to explore the evolution of cool dwarfs many times in the past, (e.g. Reid et al. 1995; Gizis et al. 2000; West et al. 2004, 2006; Schmidt et al. 2007; Faherty et al. 2009; Kiman et al. 2019). For example, West et al. (2004, 2006) used the vertical distances of stars from the Galactic mid-plane as an age proxy, and found that the fraction of magnetically active M dwarfs decreases over time. Faherty et al. (2009) used tangential velocities to infer the ages of M, L and T dwarfs, and showed that dwarfs with lower surface gravities tended to be kinematically younger, and Kiman et al. (2019) used velocity dispersion as an age proxy to explore the evolution of H $\alpha$  equivalent width (a magnetic activity indicator), in M dwarfs.

Although *vertical* velocity,  $v_z$ , is an established age proxy, it can only be calculated with full 6-dimensional position and velocity information. In fact, with full 6D phase space and an assumed Galactic potential, it is possible to calculate the dynamically-invariant vertical *action*, which may be an even better age indicator (Beane et al. 2018; Ting & Rix 2019). Unfortunately, most field stars with measured rotation periods do not have radial velocity (RV) measurements because they are relatively faint *Kepler* targets ( $\sim$ 12th-16th magnitudes). For this reason, we used velocity in the direction of galactic latitude,  $v_b$ , as a proxy for  $v_z$ . The *Kepler* field is positioned at low galactic latitude ( $b = \sim 5\text{--}20^\circ$ ), so  $v_b$  is a close (although imperfect, see appendix) approximation to  $v_z$ . Because we use  $v_b$  rather than  $v_z$  we do not calculate absolute kinematic ages using a published age–velocity dispersion relation (AVR), calibrated with vertical velocity. In the future it may be possible to account for the differences between  $v_b$  and  $v_z$ , or marginalize over missing RV measurements and the *Kepler* selection function, in order to infer the absolute ages of populations of stars. Regardless of direction however, velocity dispersion is expected to monotonically increase over time (e.g. Holmberg et al. 2009), and can therefore be used to *rank* populations of stars by age.

This paper is laid out as follows: in section 2 we describe our sample selection process and the methods used to calculate stellar velocities. In section 3 we use kinematics to investigate the relationship between stellar rotation period, age and color/T<sub>eff</sub> and interpret the results. We also examine the rotation period gap and the kinematics of

synchronized binaries. In the appendix, we establish that  $v_b$  velocity dispersion,  $\sigma_{vb}$ , can be used as an age proxy by demonstrating that neither mass-dependent heating nor the *Kepler/Gaia* selection function is observed to strongly affect our sample.

## 2. METHOD

### 2.1. The data

We used the publicly available *Kepler-Gaia* DR2 crossmatched catalog<sup>1</sup> to combine the McQuillan et al. (2014) catalog of stellar rotation periods, measured from *Kepler* light curves, with the *Gaia* DR2 catalog of parallaxes, proper motions and apparent magnitudes. Reddening and extinction from dust was calculated for each star using the Bayestar dust map implemented in the `dustmaps` Python package (M. Green 2018), and `astropy` (Astropy Collaboration et al. 2013; Price-Whelan et al. 2018). For this work, we used the precise *Gaia* DR2 photometric color,  $G_{BP} - G_{RP}$ , to estimate  $T_{\text{eff}}$  for the Kepler rotators. The calibration of this relation is described Curtis et al. (2020, in prep) and briefly summarized in the Appendix of this paper.

Photometric binaries and subgiants were removed from the McQuillan et al. (2014) sample by applying cuts to the color-magnitude diagram (CMD), shown in figure 1. A 6th-order polynomial was fit to the main sequence and raised by 0.27 dex to approximate the division between single stars and photometric binaries (shown as the curved dashed line in figure 1). All stars above this line were removed from the sample. Potential subgiants were also removed by eliminating stars brighter than 4th absolute magnitude in *Gaia* G-band. This cut also removed a number of main sequence F stars from our sample, however these hot stars are not the focus of our gyrochronology study since their small convective zones inhibit the generation of a strong magnetic field. The removal of photometric binaries and evolved/hot stars reduced the total sample of around 34,000 stars by almost 10,000.

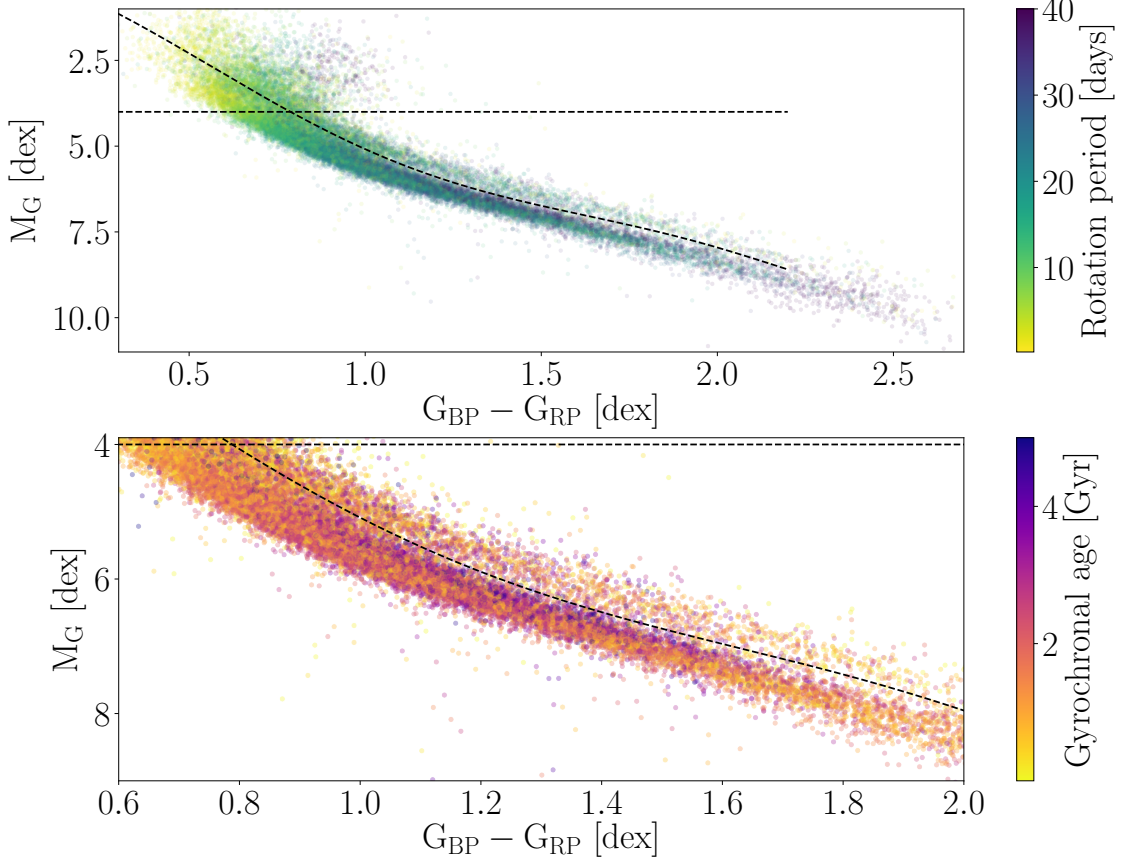
The rotation periods of the dwarf stars in the McQuillan et al. (2014) sample are shown on a *Gaia* color-magnitude diagram (CMD) in the top panel of figure 1. In the bottom panel, the stars are colored by their gyrochronal age, calculated using the Angus et al. (2019) gyrochronology relation. The stars with old gyrochronal ages, plotted in purple hues, predominantly lie along the upper edge of the MS, where stellar evolution models predict old stars to be, however the majority of these ‘old’ stars are bluer than  $G_{BP} - G_{RP} \sim 1.5$  dex. The lack of gyrochronologically old M dwarfs suggests that either old M dwarfs are missing from the McQuillan et al. (2014) catalog, or the Angus et al. (2019) gyrochronology relation under-predicts the ages of low-mass stars. Given that lower-mass stars stay active for longer than higher-mass stars (e.g. West et al. 2008; Newton et al. 2017; Kiman et al. 2019), and are therefore more likely to have measurable rotation periods at old ages, the latter scenario seems likely. However, it is also possible that the rotation periods of the oldest early M dwarfs are so long that they are not measurable with Kepler data. Ground-based rotation period measurements of mid and late M dwarfs indicate that there is an upper limit to the rotation periods of late M dwarfs of around 140 days (Newton et al. 2016, 2018), which is much longer than the longest rotation periods measured in the McQuillan et al. (2014) sample (around 70 days). The apparent lack of old gyro-ages for M dwarfs in figure 1 may be caused by a combination of ages being underestimated by a poorly calibrated model, and rotation period detection bias. The Angus et al. (2019) gyrochronology relation is a simple polynomial model, fit to the period-color relation of Praesepe. Inaccuracies at low masses are a typical feature of empirically calibrated gyrochronology models since there are no (or at least very few) old M dwarfs with rotation periods and the models are poorly calibrated for these stars.

The `Pyia` (Price-Whelan 2018) and `astropy` (Astropy Collaboration et al. 2013; Price-Whelan et al. 2018) Python packages were used to calculate velocities for the McQuillan et al. (2014) sample. `Pyia` calculates velocity samples from the full *Gaia* uncertainty covariance matrix via Monte Carlo sampling, thereby accounting for the covariances between *Gaia* positions, parallaxes and proper motions. Stars with negative parallaxes or parallax signal-to-noise ratios less than 10 (around 3,000 stars), stars fainter than 16th magnitude in *Gaia* G-band (200 stars), stars with absolute  $v_b$  uncertainties greater than 1  $\text{km s}^{-1}$  (1000 stars), and stars with galactic latitudes greater than  $15^\circ$  (5500 stars, justification provided in the appendix) were removed from the sample. Finally, we removed almost 2000 stars with rotation periods shorter than the main population of periods, since this area of the period- $T_{\text{eff}}$  diagram is sparsely populated. We removed these rapid rotators by cutting out stars with gyrochronal ages less than 0.5 Gyr (based on the Angus et al. 2019, gyro-model), because a 0.5 Gyr gyrochrone<sup>2</sup> traces the bottom edge of the main population of

<sup>1</sup> Available at [gaia-kepler.fun](http://gaia-kepler.fun)

<sup>2</sup> A gyrochrone is a gyrochronological isochrone, or a line of constant age in period- $T_{\text{eff}}$ , or period-color space.

**Figure 1.** Top: de-reddened MS *Kepler* stars with McQuillan et al. (2014) rotation periods, plotted on a *Gaia* CMD. We removed photometric binaries and subgiants from the sample by excluding stars above the dashed lines. Bottom: a zoom-in of the top panel, with stars colored by their gyrochronal age (Angus et al. 2019), instead of their rotation period. A general age gradient is visible across the main sequence. Since the Angus et al. (2019) relation predicts that the oldest stars in the McQuillan et al. (2014) sample are late-G and early-K dwarfs, it is probably under-predicting the ages of late-K and early-M dwarfs.



rotation periods. These rapidly rotating stars are likely to be either very young stars, or synchronized binaries (see section 3.2). After these cuts, around 13,000 stars out of the original  $\sim 34,000$  were included in the sample.

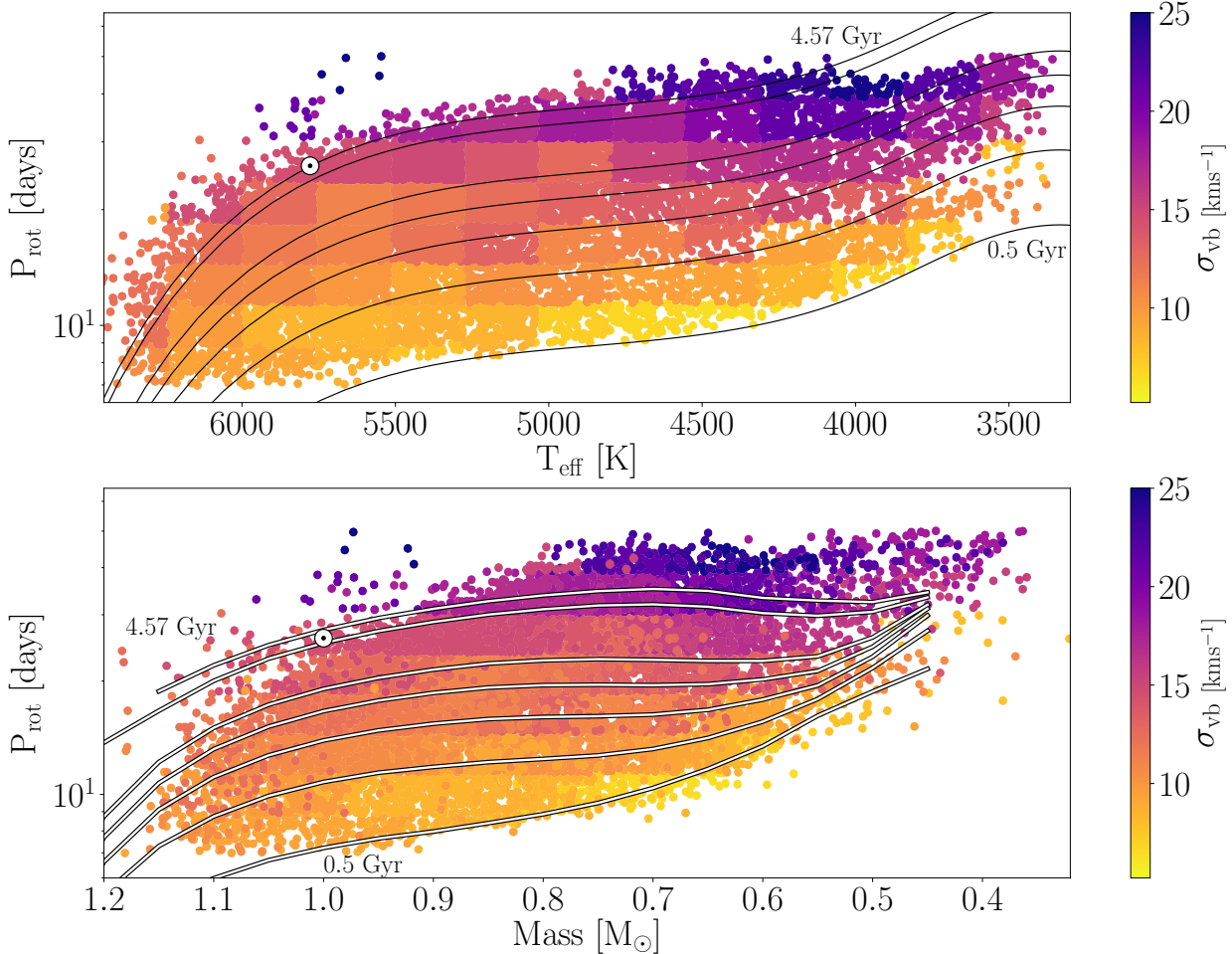
### 3. RESULTS AND DISCUSSION

#### 3.1. *The period- $T_{\text{eff}}$ relations, revealed*

To explore the relationship between rotation period, effective temperature ( $T_{\text{eff}}$ ) and velocity dispersion, we calculated  $\sigma_{v_b}$ <sup>3</sup> for populations of stars with similar rotation periods and temperatures, and presumed similar age. The top panel of figure 2 shows rotation period versus effective temperature for the McQuillan et al. (2014) sample, coloured by  $\sigma_{v_b}$ , where  $\sigma_{v_b}$  was calculated for groups of stars over a grid in  $\log_{10}(\text{period})$  and temperature. If we assume that mass dependent heating does not strongly affect this sample and  $v_b$  at low galactic latitudes is an unbiased tracer of  $v_z$ , then  $v_b$  velocity dispersion can be interpreted as an age proxy, and stars plotted in a similar color in figure 2 are similar

<sup>3</sup>  $\sigma_{v_b}$  was calculated as  $1.5 \times$  the median absolute deviation of velocities, to mitigate sensitivity to outliers.

**Figure 2.** Top: Rotation period vs effective temperature for stars in the [McQuillan et al. \(2014\)](#) sample, colored by the velocity dispersions of stars calculated over a grid in  $\log_{10}(\text{period})$  and  $T_{\text{eff}}$  (this grid causes the quantized appearance). Black lines show gyrochrones from a gyrochronology model that projects the rotation-color relation of Praesepe to longer rotation periods over time ([Angus et al. 2019](#)). These gyrochrones do not appear to reflect the evolution of field stars at long rotation periods/old ages because they do not trace lines of constant velocity dispersion. Gyrochrones are plotted at 0.5, 1, 1.5, 2, 2.5, 4 and 4.57 Gyr (Solar age) in both top and bottom panels. Bottom: Same as top panel with rotation period vs *mass* (from [Berger et al. 2020](#)). White lines show gyrochrones from a model that includes mass and age-dependent angular momentum transport between the core and envelope ([Spada & Lanzafame 2019](#)). Qualitatively, these gyrochrones reflect the evolution of field stars at long rotation periods/old ages: they trace lines of constant velocity dispersion by reproducing periods of ‘stalled’ surface rotational evolution for K-dwarfs.



ages. In the appendix of this paper, we show that this assumption appears valid for stars with Galactic latitude  $< 15^\circ$ .

Overall, figure 2 shows that velocity dispersion increases with rotation period across all temperatures, implying that rotation period increases with age, as expected. This result is insensitive to the choice of bin position and size. Black lines show gyrochrones from the [Angus et al. \(2019\)](#) gyrochronology model, which projects the rotation-color relation of Praesepe to longer rotation periods over time. These gyrochrones are plotted at 0.5, 1, 1.5, 2, 2.5, 4 and 4.57 (Solar age) Gyr. At the youngest ages, these gyrochrones describe the data well: the palest yellow (youngest) stars with the lowest velocity dispersions all fall close to the 0.5 Gyr gyrochrone. However, although the 0.5 Gyr and 1 Gyr gyrochrones also trace constant velocity dispersion/age among the field stars, by 1.5 Gyr the gyrochrones start to cross different velocity dispersion regimes. For example, the 1.5 Gyr gyrochrone lies on top of stars with velocity

dispersions of around 10-11  $\text{km s}^{-1}$  at 5000-5500K and stars with  $\sim 15 \text{ km s}^{-1}$  velocity dispersions at 4000-4500K. The gyrochrones older than 1.5 Gyr also cross a range of velocity dispersions. If these were true isochrones they would follow lines of constant velocity dispersion. At ages older than around 1 Gyr, it appears that gyrochrones should have a more flattened, or even inverted, shape in rotation period- $T_{\text{eff}}$  space than these Praesepe-based models.

The bottom panel of figure 2 shows velocity dispersion as a function of rotation period and *mass*, (from Berger et al. 2020), with gyrochrones from the Spada & Lanzafame (2019) model shown in white. These gyrochrones are plotted for the same ages as above. Each point plotted in the top panel also appears in the bottom panel with the same color. Because velocity dispersion was calculated in bins of  $T_{\text{eff}}$ , not mass, bin outlines are clearly visible in the top panel but appear smeared-out in the bottom panel. In the bottom panel of figure 2, the Spada & Lanzafame (2019) models do trace lines of constant velocity dispersion, and reproduce the trends in the data at all ages. These models qualitatively agree with the data and reproduce the apparent flattening and inversion in the rotation period- $T_{\text{eff}}$ /mass relations.

The results shown in figure 2 indicate that stars of spectral type ranging from late G to late K ( $\sim 5500$ - $3500$  K) follow a braking law that changes over time. In particular, the relationship between rotation period and effective temperature appears to flatten out and eventually invert. These results provide further evidence for ‘stalled’ surface rotational evolution of K dwarfs, like that observed in open clusters (Curtis et al. 2019) and reproduced by models that vary angular momentum transport between stellar core and envelope with time and mass (Spada & Lanzafame 2019).

In the top panel of figure 2, the Angus et al. (2019) gyrochronology model is over-plotted for comparison. We used this model as an example, however all empirical gyrochronology models are similar in essence to the Angus et al. (2019) relation and none is able to reproduce the observed velocity dispersions, or capture the evolving shape of the period- $T_{\text{eff}}$  relations. The Angus et al. (2019) relation is a new fully-empirical gyrochronology relation, calibrated using recently measured rotation periods for members of the Praesepe cluster, which extend down to early M dwarfs (Rebull et al. 2017; Douglas et al. 2017). These are the oldest cluster M dwarfs with measured photometric rotation periods and the Angus et al. (2019) model therefore encapsulates the behavior of these cool stars at Praesepe age.

Alternatively, we could have chosen to compare our data with one of the many other available empirical gyrochronology models. For example, the Barnes (2003, 2007); Mamajek & Hillenbrand (2008); Meibom et al. (2011); Angus et al. (2015) relations all have a functional form that was first introduced by Barnes (2003):  $P_{\text{rot}} = t^n a(B - V - c)^b$ , where  $n$ ,  $a$ ,  $b$  and  $c$  are free parameters, and  $B$  and  $V$  are photometric magnitudes. These relations have been widely used in the literature, and are similar to the Angus et al. (2019) relation in that they consist of a color-dependent term multiplied by an age-dependent term, *i.e.* they are separable in color and age. None of these relations follow lines of constant velocity dispersion in figure 2 because they have a universal power-law index,  $n$  (around 0.5), which applies to stars of all masses and ages. They do not have the flexibility to capture the evolving period-color relationship seen in the data. The Barnes (2010) model has a different functional form: it uses Rossby number ( $Ro = P_{\text{rot}}/\tau$ , where  $\tau$  is the convective turnover time) to encode the mass-dependent evolution of rotation periods:  $\frac{dP_{\text{rot}}}{dt} \propto 1/Ro$ . This simple relation neatly reproduces the rotation periods of young cluster stars, however, like the other empirical gyrochronology models, it does not reproduce the observed trends seen in the velocity dispersion data. It has a similar period- $T_{\text{eff}}$  relation to the Praesepe-based Angus et al. (2019) model, because the period- $T_{\text{eff}}$  relation of Praesepe roughly follows a line of constant Rossby number. Consequently, like the Angus et al. (2019) model, the Barnes (2010) gyrochrones do not reproduce the data explored here and do not have the flexibility to capture mass and time-variable rotational evolution.

The lack of flexibility that is baked-in to these empirical gyrochronology models should not be seen as a failing of gyrochronologists: with a paucity of calibration data for old stars all one can do is fit simple relations to young stars and extrapolate to old ages. Naturally however, in this era of precise space-based photometry, new data are revealing flaws in our old models (which no one ever thought were perfect), and are providing opportunities to improve them.

The velocity dispersions of stars in the McQuillan et al. (2014) sample, shown in figure 2, provide the following picture of rotational evolution. At young ages (younger than around 1 Gyr but still old enough to be on the main sequence and have transitioned from the ‘C’ sequence to the ‘I’ sequence Barnes 2003), stellar rotation period *decreases* with *increasing* mass. This is likely because lower-mass stars with deeper convection zones have stronger magnetic fields, larger Alfvén radii and therefore experience greater angular momentum loss rate (*e.g.* Schatzman 1962; Kraft 1967; Parker 1970; Kawaler 1988; Charbonneau 2010; Matt et al. 2012, 2015). According to the Spada & Lanzafame (2019) model, the radiative cores and convective envelopes of stars are decoupled at these young ages, *i.e.* transportation of angular momentum from the surface to the core of the star is reduced, so the surface slows down due to wind-braking

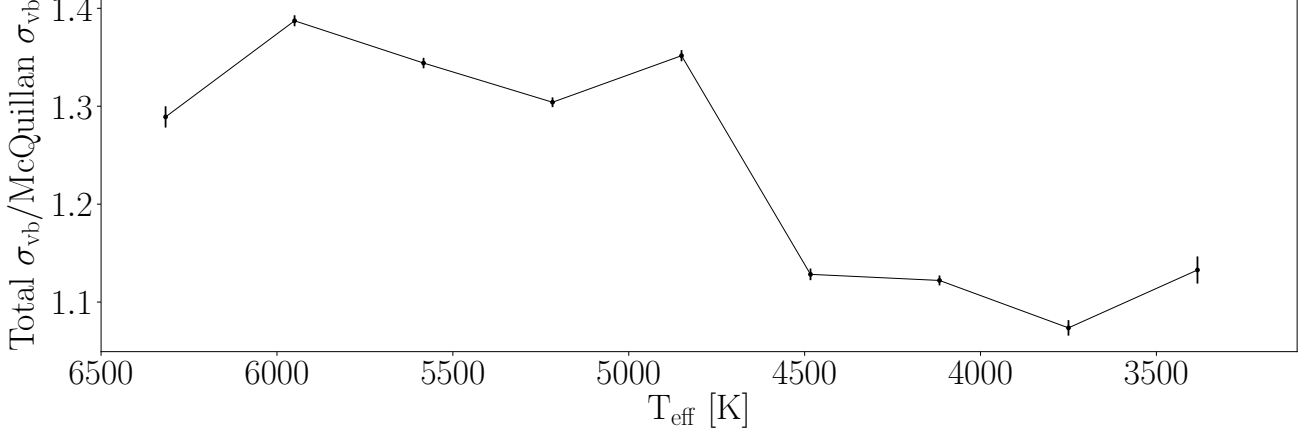
but the core keeps spinning rapidly. According to the data presented in figure 2, at intermediate ages, the rotation periods of K dwarfs appear *constant* with mass, and at late ages rotation period *increases* with *increasing* mass. The interpretation of this, according to the Spada & Lanzafame (2019) model, is that lower-mass stars are still braking more efficiently at these intermediate and old ages *compared to higher-mass stars*, but their cores are more tightly coupled to their envelopes, allowing angular momentum transport between the two layers. Angular momentum resurfaces *from the core* and prevents the stellar envelopes from spinning-down rapidly, and this effect is strongest for late K-dwarfs with effective temperatures of  $\sim$ 4000-4500K and masses  $\sim$ 0.5-0.7  $M_{\odot}$ .

A period of core-envelope decoupling in the evolution of cool dwarfs has been explored in theoretical models for decades (*e.g.* Endal & Sofia 1981; MacGregor & Brenner 1991; Denissenkov et al. 2010; Gallet & Bouvier 2013). In such models, the angular momenta of the radiative core and convective envelope are permitted to evolve separately once a radiative core develops on the pre-main sequence. A decoupled core and envelope is required to reproduce observations of young clusters and star forming regions (*e.g.* Irwin et al. 2007; Bouvier 2008; Denissenkov et al. 2010; Spada et al. 2011; Reiners & Mohanty 2012) and has become an established element of theoretical gyrochronology models. During this phase, angular momentum transport between the radiative core and the convective envelope is reduced. Over time, models increase the efficiency of angular momentum transport between the core and envelope in order to reproduce the close-to solid body rotation observed for the Sun (*e.g.* Thompson et al. 1996). The core-envelope coupling timescale affects the predicted surface rotation periods of young and intermediate-age stars and is usually constrained using observations of open clusters. The Lanzafame & Spada (2015) gyrochronology model uses a mass-dependent core-envelope coupling timescale, and Spada & Lanzafame (2019) fit this model to open-cluster observations, including new rotation period measurements for K dwarfs in the NGC 6811 cluster (Curtis et al. 2019). A similar mass-dependent core-envelope coupling timescale was also found to explain the observed lithium depletion trends in open clusters by an independent study (Somers & Pinsonneault 2016). Although variable angular momentum transport between the surfaces and cores of stars has been an essential ingredient of stellar evolution models for decades, the transport mechanism is still unknown. Among the proposed mechanisms are magneto-hydrodynamical waves resulting from various magnetic field geometries, and gravity waves (see, *e.g.* Charbonneau & MacGregor 1993; Ruediger & Kitchatinov 1996; Spruit 2002; Talon & Charbonnel 2003; Spada et al. 2010; Brun et al. 2011; Oglethorpe & Garaud 2013).

In order to measure a rotation period at all, there must be some magnetically active regions (either bright plages or dark spots), of a reasonable size on the surface of a star. The relatively sharp upper-edge of the rotation period distribution seen in figure 2 may therefore be caused by a finite active lifetime of stars. The mass dependence of magnetic activity lifetimes has been demonstrated previously for M dwarfs (*e.g.* West et al. 2008; Newton et al. 2017; Kiman et al. 2019), and if the detectability of a rotation period is considered to be a magnetic activity proxy, then our results provide further evidence for a *mass-dependent* activity lifetime. Figure 2 shows that the populations of stars with the largest velocity dispersions are cooler than 4500 K. This implies that the oldest stars with detectable rotation periods are cooler than 4500 K, *i.e.* these low mass stars stay active longer than more massive stars.

To investigate this idea further, we compared the velocity dispersions of stars with *measured rotation periods* to the velocity dispersions of the entire *Kepler* sample. If stars with measured rotation periods are more magnetically active and younger than stars without rotation period measurements, they should also have smaller velocity dispersions. To test this theory, we calculated the velocity dispersions for all stars in the *Kepler* field after removing visual binaries, subgiants, stars fainter than 16th magnitude, and high Galactic latitude stars, following the method described in section 2. We then compared these velocity dispersions, as a function of  $T_{\text{eff}}$ , to the velocity dispersions of stars with *measured* rotation periods (*i.e.* stars that appear in table 1 of McQuillan et al. 2014). We show the ratio of total  $\sigma_{vb}$  to McQuillan- $\sigma_{vb}$  as a function of  $T_{\text{eff}}$  in figure 3. A larger ratio means the rotating star sample is *younger*, on average, than the overall *Kepler* population, and a ratio of 1 means that the rotating stars have the *same* age distribution as the overall Kepler sample. Figure 3 shows that this ratio is largest for G stars and approaches unity for K and early M dwarfs. This indicates that the G stars with detectable rotation periods are, on average, *younger* than the total population of G stars in the Kepler field. On the other hand, the late K and early M dwarfs with detectable rotation periods have a similar age distribution to the overall Kepler population which suggests that the oldest K and M dwarfs are represented in the McQuillan et al. (2014) sample. This result bolsters the evidence that M dwarf rotation periods are measurable at older ages than G dwarf rotation periods. In other words, G stars become magnetically inactive and have fewer active surface regions *at a younger age than M dwarfs*.

**Figure 3.** Velocity dispersions for the entire *Kepler* field divided by the velocity dispersions of stars with measured rotation periods in McQuillan et al. (2014), as a function of effective temperature. A larger ratio indicates that the overall *Kepler* field is older, on average, than stars in the McQuillan et al. (2014) catalog. As this ratio approaches unity the two populations have similar kinematic ages. The large ratio for the hottest stars indicates that G dwarfs become inactive at young ages. This ratio approaches unity at low temperatures, showing that K and early M dwarf rotation periods are measurable over a large range of ages.



### 3.2. Synchronized binaries and the *Kepler* period gap

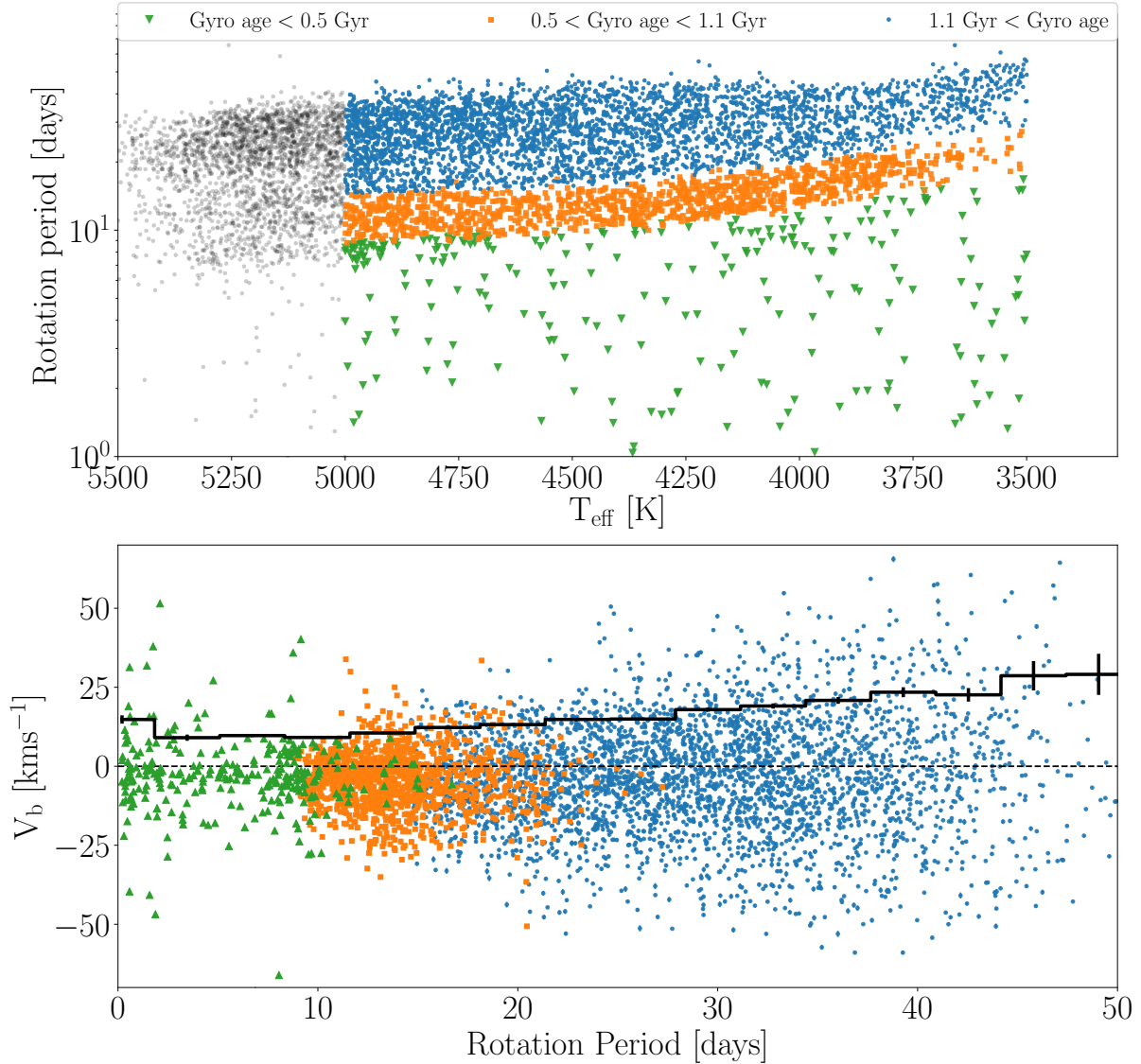
In this section, we explored the kinematic properties of the McQuillan et al. (2014) sample in more detail, investigating the velocity dispersions of stars on either side of the *Kepler* period gap, and identifying rapidly rotating stars that may be synchronized binaries.

There is a sharp gap in the population of rotation periods (often called the *Kepler* period gap), which lies just above the 1 Gyr gyrochrone in the upper panel of figure 2, whose origin is unknown and is the subject of much speculation (McQuillan et al. 2014; Davenport 2017; Davenport & Covey 2018; Reinhold et al. 2019; Reinhold & Hekker 2020). This gap was first identified by McQuillan et al. (2014), and roughly follows a line of constant gyrochronal age of around 1.1 Gyr (according to the Angus et al. 2019, gyrochronology relation). Several explanations for the gap’s origin have been proposed, including a discontinuous star formation history (McQuillan et al. 2013; Davenport 2017; Davenport & Covey 2018) and a change in magnetic field structure causing a brief period where rotational variability is reduced and rotation periods cannot be measured (Reinhold et al. 2019; Reinhold & Hekker 2020).

The top panel of figure 2 suggests that the Angus et al. (2019), Praesepe-based gyrochronology model is valid below the gap but not above. Gyrochrones follow lines of constant velocity dispersion below the gap, but cross lines of constant velocity dispersion above the gap. This phenomenon is robust to the choice of bin size and position. Although we do not provide an in-depth analysis here (and more data may be needed to confirm a connection) these data suggest that the gap may indeed separate a young regime where stellar cores are decoupled from their envelopes from an old regime where these layers are more tightly coupled. If so, this could indicate that these phenomena are related, i.e. the process that is responsible for changing the shape of gyrochrones in rotation-T<sub>eff</sub> space is related to the process that produces the gap.

An alternate explanation for the gap is that the McQuillan et al. (2014) sample contains two distinct stellar populations: one young and one old. If so, the kinematic properties of stars above and below the gap are likely to be distinctly different. The bottom panel of figure 4 shows the velocity dispersions of stars in the McQuillan et al. (2014) sample, with stars subdivided into three groups: those that rotate more quickly than the main rotation period population (green triangles), those with rotation periods shorter than the gap (orange squares), and those with rotation periods longer than the gap (blue circles). Stars were separated into these three groups using Angus et al. (2019) gyrochronology model, according to the scheme shown in the legend. Only stars cooler than 5000 K are included in the bottom panel in order to isolate populations above and below the period gap, which only extends up to a temperature of ∼4600 K in our sample, although Davenport (2017) found that the gap extends to temperatures as hot as 6000 K. In

**Figure 4.** Top: rotation period vs. effective temperature for stars in the McQuillan et al. (2014) sample, separated into three groups. Blue circles show stars with rotation periods longer than the period gap, orange squares show stars with rotation periods shorter than the gap, but longer than the lower edge of the main rotation period distribution, and green triangles show stars with rotation periods shorter than this lower edge. Stars were separated into these three groups using Angus et al. (2019) gyrochronology models, with the scheme shown in the legend. Bottom: the velocities of these groups of stars (in the direction of Galactic latitude,  $b$ ) are shown as a function of rotation period. Only stars cooler than 5000 K are plotted in the bottom panel in order to isolate populations above and below the period gap, which only extends up to temperatures of  $\sim$ 4600 K. The black line indicates the velocity standard deviation as a function of period.



general, velocity dispersion increases with rotation period because both quantities increase with age. Previously, only the overall velocity dispersions of all stars above and below the gap have been compared, leading to the assumption that these groups belong to two distinct populations (McQuillan et al. 2014). However, figure 4 shows a smooth increase in velocity dispersion with rotation period across the gap (from orange squares to blue circles), suggesting that these groups are part of the same Galactic population. This observation does not rule out the possibility that a brief cessation of star formation in the Solar neighborhood, around one Gyr ago, may have caused this gap, however.

In the final part of our analysis, we investigated the potential for using kinematics to identify synchronized binaries in the McQuillan et al. (2014) sample. Synchronized binaries are pairs of stars whose rotation periods are equal to their orbital period. Since synchronization appears to happen at rotation periods of 7 days or shorter (Simonian et al. 2019), and most isolated stars have rotation periods longer than 7 days, the rotation periods of synchronized binaries are likely to be *shorter* than they would be if they were isolated stars. For this reason, their rotation periods do not reflect their ages and the gyrochronal age of a synchronized binary is likely to be much younger than the true age of the system. Synchronized binaries are therefore a source of contamination for gyrochronology and should be removed from samples before performing a gyrochronal age analysis. Figure 4 shows that some of the most rapidly rotating stars in the McQuillan et al. (2014) sample have relatively large absolute velocities, indicating that they are likely synchronized binaries. For this reason, the velocity dispersions of stars with rotation periods shorter than the lower edge of the rotation period distribution (green triangles in figure 4) are not significantly smaller than the, presumed older, orange-colored stars. In general, stars with rotation periods less than  $\sim 10$  days have an increased chance of being synchronized binaries. This result is in agreement with a recent study which found that a large fraction of photometric binaries were rapid rotators, and the probability of a star being a synchronized binary system substantially increased below rotation periods of around 7 days (Simonian et al. 2019). We caution users of rotation period catalogs that rapid rotators with large absolute velocities should be flagged as potential synchronized binaries before applying any gyrochronal analysis.

#### 4. CONCLUSIONS

In this paper, we used the  $v_b$  velocity dispersions of stars in the McQuillan et al. (2014) catalog to explore the evolution of stellar rotation period as a function of effective temperature and age. Our conclusions are as follows:

- **Spin-down rate doesn't always increase with decreasing mass for K dwarfs.** Although at young ages, rotation period is anti-correlated with  $T_{\text{eff}}$  (as seen in many young open clusters, including Praesepe), at intermediate ages the relation flattens out and K dwarfs of different masses rotate at the same rate. At old ages, cooler K dwarfs spin more rapidly than hotter K dwarfs of the same age.
- **Variable core-envelope coupling may be the cause.** We showed that the period– $T_{\text{eff}}$  relations change shape over time in a way that qualitatively agrees with theoretical models which include mass and time-dependent core-envelope angular momentum transport (Spada & Lanza 2019).
- **Low-mass stars stay active longer.** We found that the oldest stars in the McQuillan et al. (2014) catalog are cooler than 4500 K, which agrees with previous results which show that lower-mass stars remain active for longer, allowing their rotation periods to be measured at older ages.
- **The Kepler period gap may be related to core-envelope coupling.** We speculated that the rotation period gap (McQuillan et al. 2014) may separate a young regime where stellar rotation periods decrease with increasing mass from an old regime where periods increase with increasing mass, however more data are needed to provide a conclusive result. The velocity dispersions of stars increase smoothly across the rotation period gap, indicating that the gap does not separate two distinct stellar populations.
- **Rapidly rotating stars with large absolute velocities may be synchronized binaries.** We used kinematics to indicate that there is a population of synchronized binaries with rotation periods less than around 10 days.

We would like to thank Suzanne Aigrain for providing thoughtful insight that improved this paper. This work was partly developed at the 2019 KITP conference ‘Better stars, better planets’. This research was supported in part by the National Science Foundation under Grant No. NSF PHY-1748958. Parts of this project are based on ideas

explored at the Gaia sprints at the Flatiron Institute in New York City, 2016 and MPIA, Heidelberg, 2017. This work made use of the `gaia-kepler.fun` crossmatch database created by Megan Bedell.

Some of the data presented in this paper were obtained from the Mikulski Archive for Space Telescopes (MAST). STScI is operated by the Association of Universities for Research in Astronomy, Inc., under NASA contract NAS5-26555. Support for MAST for non-HST data is provided by the NASA Office of Space Science via grant NNX09AF08G and by other grants and contracts. This paper includes data collected by the Kepler mission. Funding for the *Kepler* mission is provided by the NASA Science Mission directorate.

This work has made use of data from the European Space Agency (ESA) mission *Gaia* (<https://www.cosmos.esa.int/gaia>), processed by the *Gaia* Data Processing and Analysis Consortium (DPAC, <https://www.cosmos.esa.int/web/gaia/dpac/consortium>). Funding for the DPAC has been provided by national institutions, in particular the institutions participating in the *Gaia* Multilateral Agreement.

## 5. APPENDIX A: VALIDATING $v_b$ DISPERSION AS AN AGE PROXY

The conclusions drawn in this paper depend on the assumption that velocity dispersion in the direction of Galactic latitude ( $\sigma_{v_b}$ ) can be used as an age proxy. There are two main reasons however, why  $v_b$  velocity dispersion may *not* be a good age proxy. Firstly, mass-dependent heating may act on the sample, meaning that velocity dispersion depends on both age and mass. Secondly, since stars in the *Kepler* field have a range of Galactic latitudes, using  $v_b$  as a stand-in for  $v_z$  may not be equally valid for all stars, and introduce a velocity bias for high latitude stars (which are more likely to be cooler and older). In this section we demonstrate that neither of these problems seem to be a significant issue for our data.

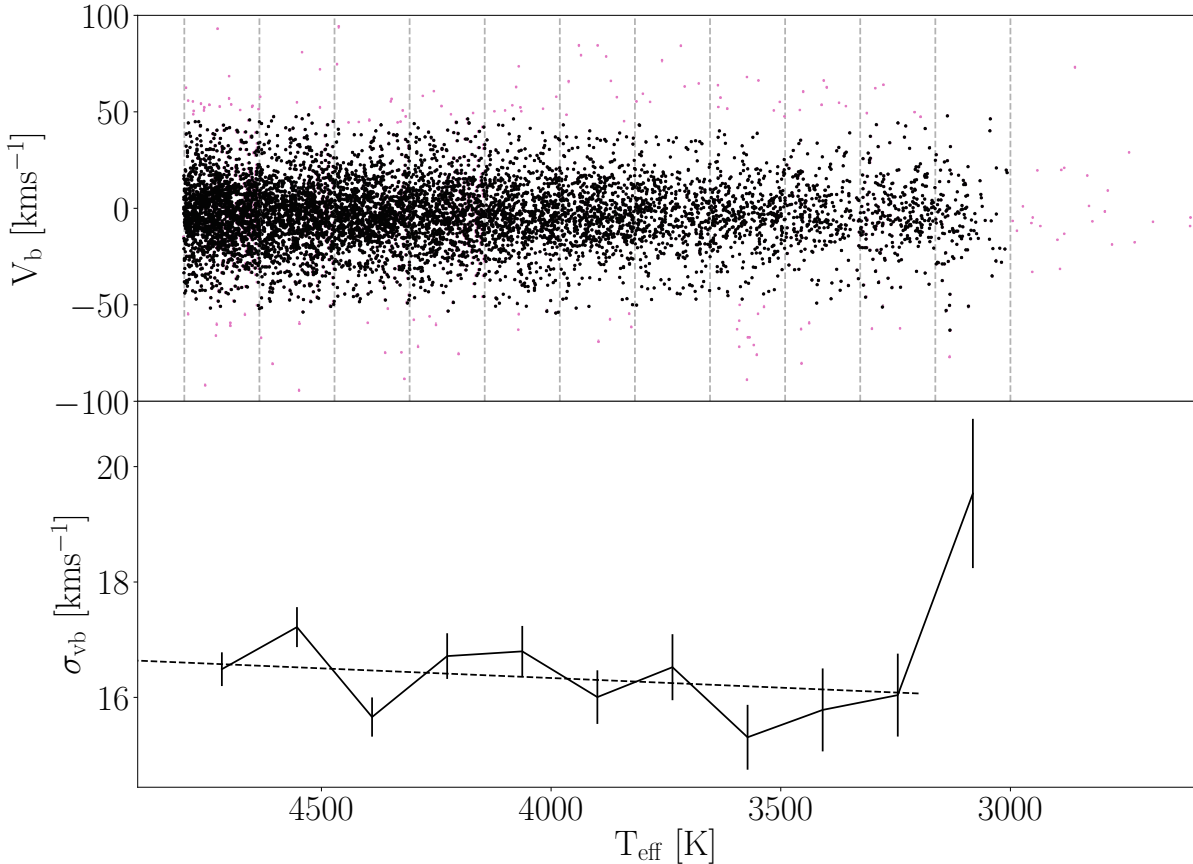
In order to establish whether  $\sigma_{v_b}$  can be used as an age proxy, we searched for signs of mass-dependent heating within the *Kepler* field. Mass-dependent dynamical heating may result from lower-mass stars experiencing greater velocity changes when gravitationally perturbed than more massive stars. It has not been unambiguously observed in the galactic disk because of the strong anti-correlation between stellar mass and stellar age. Less massive stars do indeed have larger velocity dispersions, however they are also older on average. This mass-age degeneracy is highly reduced in M dwarfs because their main-sequence lifetimes are longer than the age of the Universe, and no evidence for mass-dependent heating has previously been found in M dwarfs (e.g. Faherty et al. 2009; Newton et al. 2016).

To investigate whether mass-dependent heating could be acting on the *Kepler* sample, we selected late K and early M dwarfs observed by both *Kepler* and *Gaia*, whose MS lifetimes exceed around 11 Gyr and are therefore representative of the initial mass function. We could not perform this analysis on the McQuillan et al. (2014) sample, because it only includes stars with *detectable* rotation periods, and since lower-mass stars stay active for longer it is likely that it contains a strong mass-age correlation. We selected all *Kepler* targets with dereddened *Gaia*  $G_{BP} - G_{RP}$  colors greater than 1.2 (corresponding to an effective temperature  $\lesssim 4800$  K) and absolute *Gaia*  $G$ -band magnitudes  $> 4$ . We also eliminated photometric binaries by removing stars above a 6th order polynomial, fit to the MS on the *Gaia* CMD (similar to the one shown in figure 1). We then applied the quality cuts described above in section 2.1. To search for evidence of mass-dependent heating we calculated the ( $v_b$ ) velocity dispersion of stars in effective temperature bins. Sigma clipping was performed at  $3\sigma$  to remove high and low velocity outliers before calculating the standard deviation of stars in each bin. These extreme velocity outliers may be very old late K and early M dwarfs, or they result from using  $v_b$  instead of  $v_z$ , which introduces additional velocity scatter.

Figure 5 shows velocity and velocity dispersion as a function of effective temperature for the K and M *Kepler* dwarf sample. Velocity dispersion very slightly *decreases* with decreasing temperature, the opposite of the trend expected for mass-dependent heating, however the slope is only inconsistent with zero at  $1.3\sigma$ . The sharp uptick in velocity dispersion in the coolest bin is probably noise caused by the small number of stars in that bin. This trend may be due to a selection bias: cooler stars are fainter and therefore typically closer, with smaller heights above the galactic plane and smaller velocities. The essential point however, is that we do not see evidence for mass-dependent heating acting on stars in the *Kepler* field, indicating that velocity dispersion *can* be used as an age proxy (with the caveat that there is still a chance, albeit a small one, that the opposing effects of the selection function and mass-dependent heating are working to cancel each other out). This analysis was performed using  $v_b$  but we also examined the *vertical* velocities of the 537 stars in this sample with RV measurements. Again, no evidence was found for mass-dependent heating: the slope of the velocity dispersion-temperature relation was consistent with zero.

Having found no strong evidence for mass-dependent heating, we next tested the validity of  $v_b$  as a proxy for  $v_z$  in more detail. At a galactic latitude,  $b$ , of zero,  $v_b = v_z$ , however for increasing values of  $b$ , this equivalence becomes an

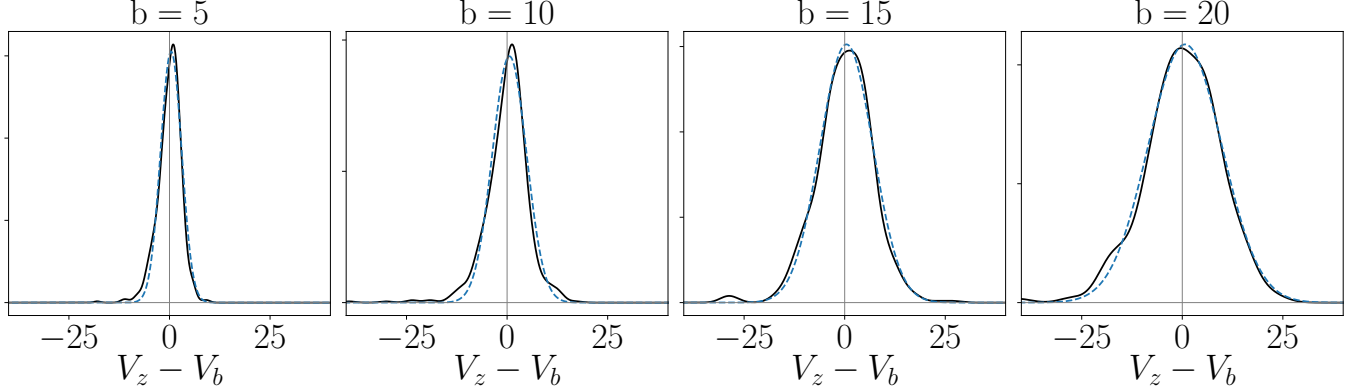
**Figure 5.** Top: Stellar velocity ( $v_b$ ) as a function of  $T_{\text{eff}}$  for *Kepler* K and M dwarfs. Vertical lines indicate different  $T_{\text{eff}}$ -groupings used to calculate velocity dispersion. Pink stars were not included in velocity dispersion calculations as they were either removed as outliers during a sigma clipping process, or they lie at the sparsely populated, extremely cool end of the temperature range. Velocity dispersion and  $T_{\text{eff}}$  are slightly positively correlated, likely due to a brightness-related selection bias, indicating that mass-dependent heating does not significantly affect low-mass stars in the *Kepler* field.



approximation that grows noisier with  $b$ . To test the validity of the  $v_b \sim v_z$  approximation over a range of latitudes we downloaded stellar data from the *Gaia* Universe Model Snapshot (GUMS) simulation – a simulated *Gaia* catalog (Robin et al. 2012). We downloaded stars from four pointings in the *Kepler* field with galactic latitudes of around 5°, 10°, 15°, and 20°, out to a limiting magnitude of 16 dex, and calculated their  $v_z$  and  $v_b$  velocities. The relationship between  $v_z$  and  $v_b$  is close to 1:1, with  $v_z$  greater than  $v_b$  by around 4.5 km s $^{-1}$  at  $b = 5$ , due to the Sun’s own motion in the Galaxy. We subtracted this offset and examined the residuals of the  $v_z - v_b$  relationship to investigate the variance as a function of Galactic latitude (shown in figure 6). We found that  $v_b$  is drawn from a heavy-tailed distribution, centered on  $v_z$ , with standard deviation increasing with  $b$  (see figure 6). The standard deviation of  $v_z - v_b$  was around 3 km s $^{-1}$  at  $b \sim 5^\circ$ , 4 km s $^{-1}$  at  $10^\circ$ , 6 km s $^{-1}$  at  $15^\circ$ , and 9 km s $^{-1}$  at  $20^\circ$ . This demonstrates that using  $v_b$  instead of  $v_z$  for stars in the *Kepler* field will introduce an additional velocity scatter, inflating  $\sigma_{v_b}$  relative to  $\sigma_{v_z}$ . This additional velocity scatter will be greatest for stars at the highest Galactic latitudes.

Since we are concerned with velocity *dispersions*, rather than velocities themselves, we also compared  $\sigma_{v_b}$  and  $\sigma_{v_z}$  as a function of temperature for stars downloaded from the GUMS simulation. For stars at galactic latitudes of 15° or less,  $\sigma_{v_b}$  was consistent with  $\sigma_{v_z}$ , within uncertainties, however, at higher latitudes the two quantities became significantly different. For this reason we proceeded by only including stars with galactic latitudes less than 15° in

**Figure 6.** This figure demonstrates the variance in the relationship between  $v_b$  and  $v_z$  for stars in the *Kepler* field, based on the GUMS simulation. The panels show a kernel density estimator (KDE) (black solid line) for the  $v_z - v_b$  residuals of stars in the GUMS simulation at four different Galactic latitudes. Blue dashed lines show Gaussian fits to these KDEs. The distributions are close to Gaussian, with slightly heavy tails. The standard deviations of the Gaussian fits increase with Galactic latitude. This figure illustrates how using  $v_b$  instead of  $v_z$  artificially increases velocity dispersion, especially at high latitudes.



our analysis. Although we find that the transformation between  $v_z$  and  $v_b$  does not *strongly* affect our results, we cannot rule out the possibility that it introduces systematic biases into the velocity dispersions we present here. In *Gaia* DR3, RVs will be available for most stars in this sample, providing an opportunity to validate (or correct) the results presented here, and to work in action-space, rather than velocity-space.

Because of the noisy relationship between  $v_b$  and  $v_z$  in this paper we do not attempt to convert velocity dispersion ( $\sigma_{v_b}$ ) into an age via an age-velocity dispersion relation (AVR) (e.g. Holmberg et al. 2009). Although we find that  $\sigma_{v_b}$  can be used to rank populations of stars by age, a more careful analysis that includes formal modeling of the  $v_b - v_z$  relationship will be needed to calculate absolute ages.

## 6. APPENDIX B: PHOTOMETRIC TEMPERATURES

For this work, we used the precise *Gaia* DR2 photometric color,  $G_{\text{BP}} - G_{\text{RP}}$ , to estimate  $T_{\text{eff}}$  for the Kepler rotators. To calibrate this relation, Curtis et al. (2020, in prep) combined effective temperature measurements for nearby, unreddened field stars in benchmark samples, including FGK stars characterized with high-resolution optical spectroscopy (Brewer et al. 2016), M dwarfs characterized with low-resolution optical and near-infrared spectroscopy (Mann et al. 2015), and K and M dwarfs characterized with interferometry and bolometric flux analyses (Boyajian et al. 2012). This empirical color–temperature relation is valid over the color range  $0.55 < (G_{\text{BP}} - G_{\text{RP}})_0 < 3.20$ , corresponding to  $3070 > T_{\text{eff}} > 6470$  K. The dispersion about the relation implies a high precision of 50 K. These benchmark data enable us to accurately estimate  $T_{\text{eff}}$  for cool dwarfs (e.g. Rabus et al. 2019), and allows us to correct for interstellar reddening at all temperatures<sup>4</sup>. The equation we used to calculate photometric temperatures from *Gaia*  $G_{\text{BP}} - G_{\text{RP}}$  color is a seventh-order polynomial with coefficients given in table 1.

## REFERENCES

- Angus, R., Aigrain, S., & Foreman-Mackey et al, D. 2015, MNRAS, 450, 1787, doi: [10.1093/mnras/stv423](https://doi.org/10.1093/mnras/stv423)
- Angus, R., Morton, T. D., & Foreman-Mackey et al, D. 2019, AJ, 158, 173, doi: [10.3847/1538-3881/ab3c53](https://doi.org/10.3847/1538-3881/ab3c53)
- Astropy Collaboration, Robitaille, T. P., & Tollerud et al, E. J. 2013, A&A, 558, A33, doi: [10.1051/0004-6361/201322068](https://doi.org/10.1051/0004-6361/201322068)
- Aumer, M., Binney, J., & Schönrich, R. 2016, MNRAS, 462, 1697, doi: [10.1093/mnras/stw1639](https://doi.org/10.1093/mnras/stw1639)
- Aumer, M., & Binney, J. J. 2009, MNRAS, 397, 1286, doi: [10.1111/j.1365-2966.2009.15053.x](https://doi.org/10.1111/j.1365-2966.2009.15053.x)
- Barnes, S. A. 2003, ApJ, 586, 464, doi: [10.1086/367639](https://doi.org/10.1086/367639)

<sup>4</sup> The color–temperature relation is described in detail in the Appendix of, and the formula is provided in Table 4 of, Curtis et al. (2020, in prep).

**Table 1.** Coefficient values for the 7th-order polynomial used to estimate  $T_{\text{eff}}$  from *Gaia*  $G_{BP} - G_{RP}$  color, calibrated in Curtis *et al.* (2020, in prep).

$(G_{BP} - G_{RP})$ exponent	Coefficient
0	-416.585
1	39780.0
2	-84190.5
3	85203.9
4	-48225.9
5	15598.5
6	-2694.76
7	192.865

- . 2007, ApJ, 669, 1167, doi: [10.1086/519295](https://doi.org/10.1086/519295)
- . 2010, ApJ, 722, 222, doi: [10.1088/0004-637X/722/1/222](https://doi.org/10.1088/0004-637X/722/1/222)
- Beane, A., Ness, M. K., & Bedell, M. 2018, ApJ, 867, 31, doi: [10.3847/1538-4357/aae07f](https://doi.org/10.3847/1538-4357/aae07f)
- Berger, T. A., Huber, D., & van Saders *et al.*, J. L. 2020, arXiv e-prints, arXiv:2001.07737. <https://arxiv.org/abs/2001.07737>
- Bird, J. C., Kazantzidis, S., & Weinberg *et al.*, D. H. 2013, ApJ, 773, 43, doi: [10.1088/0004-637X/773/1/43](https://doi.org/10.1088/0004-637X/773/1/43)
- Borucki, W. J., Koch, D., & Basri *et al.*, G. 2010, Science, 327, 977, doi: [10.1126/science.1185402](https://doi.org/10.1126/science.1185402)
- Bouvier, J. 2008, A&A, 489, L53, doi: [10.1051/0004-6361:200810574](https://doi.org/10.1051/0004-6361:200810574)
- Boyajian, T. S., von Braun, K., & van Belle *et al.*, G. 2012, ApJ, 757, 112, doi: [10.1088/0004-637X/757/2/112](https://doi.org/10.1088/0004-637X/757/2/112)
- Brewer, J. M., Fischer, D. A., & Valenti *et al.*, J. A. 2016, ApJS, 225, 32, doi: [10.3847/0067-0049/225/2/32](https://doi.org/10.3847/0067-0049/225/2/32)
- Brun, A. S., Miesch, M. S., & Toomre, J. 2011, ApJ, 742, 79, doi: [10.1088/0004-637X/742/2/79](https://doi.org/10.1088/0004-637X/742/2/79)
- Casagrande, L., Schönrich, R., & Asplund *et al.*, M. 2011, A&A, 530, A138, doi: [10.1051/0004-6361/201016276](https://doi.org/10.1051/0004-6361/201016276)
- Charbonneau, P. 2010, Living Reviews in Solar Physics, 7, 3, doi: [10.12942/lrsp-2010-3](https://doi.org/10.12942/lrsp-2010-3)
- Charbonneau, P., & MacGregor, K. B. 1993, ApJ, 417, 762, doi: [10.1086/173357](https://doi.org/10.1086/173357)
- Curtis, J. L., Agüeros, M. A., & Douglas *et al.*, S. 2019, arXiv e-prints. <https://arxiv.org/abs/1905.06869>
- Davenport, J. R. A. 2017, ApJ, 835, 16, doi: [10.3847/1538-4357/835/1/16](https://doi.org/10.3847/1538-4357/835/1/16)
- Davenport, J. R. A., & Covey, K. R. 2018, ApJ, 868, 151, doi: [10.3847/1538-4357/aae842](https://doi.org/10.3847/1538-4357/aae842)
- Denissenkov, P. A., Pinsonneault, M., & Terndrup *et al.*, D. M. 2010, ApJ, 716, 1269, doi: [10.1088/0004-637X/716/2/1269](https://doi.org/10.1088/0004-637X/716/2/1269)
- Douglas, S. T., Agüeros, M. A., & Covey *et al.*, K. R. 2017, ApJ, 842, 83, doi: [10.3847/1538-4357/aa6e52](https://doi.org/10.3847/1538-4357/aa6e52)
- Endal, A. S., & Sofia, S. 1981, ApJ, 243, 625, doi: [10.1086/158628](https://doi.org/10.1086/158628)
- Faherty, J. K., Burgasser, A. J., & Cruz *et al.*, K. L. 2009, AJ, 137, 1, doi: [10.1088/0004-6256/137/1/1](https://doi.org/10.1088/0004-6256/137/1/1)
- Gallet, F., & Bouvier, J. 2013, A&A, 556, A36, doi: [10.1051/0004-6361/201321302](https://doi.org/10.1051/0004-6361/201321302)
- García, R. A., Ceillier, T., & Salabert *et al.*, D. 2014, A&A, 572, A34, doi: [10.1051/0004-6361/201423888](https://doi.org/10.1051/0004-6361/201423888)
- Gizis, J. E., Monet, D. G., & Reid *et al.* 2000, AJ, 120, 1085, doi: [10.1086/301456](https://doi.org/10.1086/301456)
- Holmberg, J., Nordström, B., & Andersen, J. 2007, A&A, 475, 519, doi: [10.1051/0004-6361:20077221](https://doi.org/10.1051/0004-6361:20077221)
- . 2009, A&A, 501, 941, doi: [10.1051/0004-6361/200811191](https://doi.org/10.1051/0004-6361/200811191)
- Howell, S. B., Sobeck, C., & Haas *et al.*, M. 2014, PASP, 126, 398, doi: [10.1086/676406](https://doi.org/10.1086/676406)
- Irwin, J., & Bouvier, J. 2009, in IAU Symposium, Vol. 258, The Ages of Stars, ed. E. E. Mamajek, D. R. Soderblom, & R. F. G. Wyse, 363–374, doi: [10.1017/S1743921309032025](https://doi.org/10.1017/S1743921309032025)
- Irwin, J., Hodgkin, S., & Aigrain *et al.*, S. 2007, MNRAS, 377, 741, doi: [10.1111/j.1365-2966.2007.11640.x](https://doi.org/10.1111/j.1365-2966.2007.11640.x)
- Janes, K. A., & Hoq, S. 2011, AJ, 141, 92, doi: [10.1088/0004-6256/141/3/92](https://doi.org/10.1088/0004-6256/141/3/92)
- Kawaler, S. D. 1988, ApJ, 333, 236, doi: [10.1086/166740](https://doi.org/10.1086/166740)
- Kiman, R., Schmidt, S. J., & Angus *et al.*, R. 2019, AJ, 157, 231, doi: [10.3847/1538-3881/ab1753](https://doi.org/10.3847/1538-3881/ab1753)
- Kraft, R. P. 1967, ApJ, 150, 551, doi: [10.1086/149359](https://doi.org/10.1086/149359)
- Lanzafame, A. C., & Spada, F. 2015, A&A, 584, A30, doi: [10.1051/0004-6361/201526770](https://doi.org/10.1051/0004-6361/201526770)
- M. Green, G. 2018, The Journal of Open Source Software, 3, 695, doi: [10.21105/joss.00695](https://doi.org/10.21105/joss.00695)
- MacGregor, K. B., & Brenner, M. 1991, ApJ, 376, 204, doi: [10.1086/170269](https://doi.org/10.1086/170269)
- Mamajek, E. E., & Hillenbrand, L. A. 2008, ApJ, 687, 1264, doi: [10.1086/591785](https://doi.org/10.1086/591785)

- Mann, A. W., Feiden, G. A., & Gaidos *et al.* E. 2015, ApJ, 804, 64, doi: [10.1088/0004-637X/804/1/64](https://doi.org/10.1088/0004-637X/804/1/64)
- Martig, M., Minchev, I., & Flynn, C. 2014, MNRAS, 443, 2452, doi: [10.1093/mnras/stu1322](https://doi.org/10.1093/mnras/stu1322)
- Matt, S. P., Brun, A. S., & Baraffe *et al.* I. 2015, ApJL, 799, L23, doi: [10.1088/2041-8205/799/2/L23](https://doi.org/10.1088/2041-8205/799/2/L23)
- Matt, S. P., MacGregor, K. B., & Pinsonneault *et al.* M. H. 2012, ApJL, 754, L26, doi: [10.1088/2041-8205/754/2/L26](https://doi.org/10.1088/2041-8205/754/2/L26)
- McQuillan, A., Aigrain, S., & Mazeh, T. 2013, MNRAS, 432, 1203, doi: [10.1093/mnras/stt536](https://doi.org/10.1093/mnras/stt536)
- McQuillan, A., Mazeh, T., & Aigrain, S. 2014, ApJS, 211, 24, doi: [10.1088/0067-0049/211/2/24](https://doi.org/10.1088/0067-0049/211/2/24)
- Meibom, S., Barnes, S. A., & Latham *et al.* D. W. 2011, ApJL, 733, L9, doi: [10.1088/2041-8205/733/1/L9](https://doi.org/10.1088/2041-8205/733/1/L9)
- Meibom, S., Barnes, S. A., & Platais *et al.* I. 2015, Nature, 517, 589, doi: [10.1038/nature14118](https://doi.org/10.1038/nature14118)
- Metcalfe, T. S., & Egeland, R. 2019, ApJ, 871, 39, doi: [10.3847/1538-4357/aaf575](https://doi.org/10.3847/1538-4357/aaf575)
- Newton, E. R., Irwin, J., & Charbonneau *et al.* D. 2016, ApJ, 821, 93, doi: [10.3847/0004-637X/821/2/93](https://doi.org/10.3847/0004-637X/821/2/93)
- . 2017, ApJ, 834, 85, doi: [10.3847/1538-4357/834/1/85](https://doi.org/10.3847/1538-4357/834/1/85)
- Newton, E. R., Mondrik, N., & Irwin *et al.* J. 2018, AJ, 156, 217, doi: [10.3847/1538-3881/aad73b](https://doi.org/10.3847/1538-3881/aad73b)
- Nordström, B., Mayor, M., & Andersen *et al.* J. 2004, A&A, 418, 989, doi: [10.1051/0004-6361:20035959](https://doi.org/10.1051/0004-6361:20035959)
- Oglethorpe, R. L. F., & Garaud, P. 2013, ApJ, 778, 166, doi: [10.1088/0004-637X/778/2/166](https://doi.org/10.1088/0004-637X/778/2/166)
- Parker, E. N. 1970, ApJ, 162, 665, doi: [10.1086/150697](https://doi.org/10.1086/150697)
- Pinsonneault, M. H., Kawaler, S. D., & Sofia *et al.* S. 1989, ApJ, 338, 424, doi: [10.1086/167210](https://doi.org/10.1086/167210)
- Price-Whelan, A. 2018, doi: [10.5281/zenodo.1228136](https://doi.org/10.5281/zenodo.1228136)
- Price-Whelan, A. M., Sipőcz, B. M., & Günther *et al.* H. M. 2018, AJ, 156, 123, doi: [10.3847/1538-3881/aabc4f](https://doi.org/10.3847/1538-3881/aabc4f)
- Rabus, M., Lachaume, R., & Jordán *et al.* A. 2019, MNRAS, 484, 2674, doi: [10.1093/mnras/sty3430](https://doi.org/10.1093/mnras/sty3430)
- Rebull, L. M., Stauffer, J. R., & Hillenbrand *et al.* L. A. 2017, ApJ, 839, 92, doi: [10.3847/1538-4357/aa6aa4](https://doi.org/10.3847/1538-4357/aa6aa4)
- Reid, I. N., Hawley, S. L., & Gizis, J. E. 1995, AJ, 110, 1838, doi: [10.1086/117655](https://doi.org/10.1086/117655)
- Reiners, A., & Mohanty, S. 2012, ApJ, 746, 43, doi: [10.1088/0004-637X/746/1/43](https://doi.org/10.1088/0004-637X/746/1/43)
- Reinhold, T., Bell, K. J., & Kuszlewicz *et al.* J. 2019, A&A, 621, A21, doi: [10.1051/0004-6361/201833754](https://doi.org/10.1051/0004-6361/201833754)
- Reinhold, T., & Hekker, S. 2020, A&A, 635, A43, doi: [10.1051/0004-6361/201936887](https://doi.org/10.1051/0004-6361/201936887)
- Robin, A. C., Luri, X., & Reylé *et al.* C. 2012, A&A, 543, A100, doi: [10.1051/0004-6361/201118646](https://doi.org/10.1051/0004-6361/201118646)
- Ruediger, G., & Kitchatinov, L. L. 1996, ApJ, 466, 1078, doi: [10.1086/177577](https://doi.org/10.1086/177577)
- Sandquist, E. L., Jessen-Hansen, J., & Shetrone *et al.* M. D. 2016, ApJ, 831, 11, doi: [10.3847/0004-637X/831/1/11](https://doi.org/10.3847/0004-637X/831/1/11)
- Schatzman, E. 1962, Annales d’Astrophysique, 25, 18
- Schmidt, S. J., Cruz, K. L., & Bongiorno *et al.* 2007, AJ, 133, 2258, doi: [10.1086/512158](https://doi.org/10.1086/512158)
- Sellwood, J. A. 2014, Reviews of Modern Physics, 86, 1, doi: [10.1103/RevModPhys.86.1](https://doi.org/10.1103/RevModPhys.86.1)
- Simonian, G. V. A., Pinsonneault, M. H., & Terndrup, D. M. 2019, ApJ, 871, 174, doi: [10.3847/1538-4357/aaf97c](https://doi.org/10.3847/1538-4357/aaf97c)
- Skumanich, A. 1972, ApJ, 171, 565, doi: [10.1086/151310](https://doi.org/10.1086/151310)
- Somers, G., & Pinsonneault, M. H. 2016, ApJ, 829, 32, doi: [10.3847/0004-637X/829/1/32](https://doi.org/10.3847/0004-637X/829/1/32)
- Spada, F., & Lanza, F. 2019, arXiv e-prints, arXiv:1908.00345. <https://arxiv.org/abs/1908.00345>
- Spada, F., Lanza, F., & Lanza, A. F. 2010, MNRAS, 404, 641, doi: [10.1111/j.1365-2966.2010.16325.x](https://doi.org/10.1111/j.1365-2966.2010.16325.x)
- Spada, F., Lanza, F., & Lanza *et al.* A. F. 2011, MNRAS, 416, 447, doi: [10.1111/j.1365-2966.2011.19052.x](https://doi.org/10.1111/j.1365-2966.2011.19052.x)
- Spruit, H. C. 2002, A&A, 381, 923, doi: [10.1051/0004-6361:20011465](https://doi.org/10.1051/0004-6361:20011465)
- Stark, A. A., & Brand, J. 1989, ApJ, 339, 763, doi: [10.1086/167334](https://doi.org/10.1086/167334)
- Stark, A. A., & Lee, Y. 2005, ApJL, 619, L159, doi: [10.1086/427936](https://doi.org/10.1086/427936)
- Talon, S., & Charbonnel, C. 2003, A&A, 405, 1025, doi: [10.1051/0004-6361:20030672](https://doi.org/10.1051/0004-6361:20030672)
- Thompson, M. J., Toomre, J., & Anderson *et al.* E. R. 1996, Science, 272, 1300, doi: [10.1126/science.272.5266.1300](https://doi.org/10.1126/science.272.5266.1300)
- Ting, Y.-S., & Rix, H.-W. 2019, ApJ, 878, 21, doi: [10.3847/1538-4357/ab1ea5](https://doi.org/10.3847/1538-4357/ab1ea5)
- van Saders, J. L., Ceillier, T., & Metcalfe *et al.* T. S. 2016, Nature, 529, 181, doi: [10.1038/nature16168](https://doi.org/10.1038/nature16168)
- van Saders, J. L., Pinsonneault, M. H., & Barbieri, M. 2018, ArXiv e-prints. <https://arxiv.org/abs/1803.04971>
- Weber, E. J., & Davis, Jr., L. 1967, ApJ, 148, 217, doi: [10.1086/149138](https://doi.org/10.1086/149138)
- West, A. A., Bochanski, J. J., & Hawley *et al.* S. L. 2006, AJ, 132, 2507, doi: [10.1086/508652](https://doi.org/10.1086/508652)
- West, A. A., Hawley, S. L., & Bochanski *et al.* J. J. 2008, AJ, 135, 785, doi: [10.1088/0004-6256/135/3/785](https://doi.org/10.1088/0004-6256/135/3/785)
- West, A. A., Hawley, S. L., & Walkowicz *et al.* L. M. 2004, AJ, 128, 426, doi: [10.1086/421364](https://doi.org/10.1086/421364)